The young Galactic cluster NGC 225: binary stars' content and total mass estimate

L. Yalyalieva,[1,2,3]★ G. Carraro [ID],[3] E. Glushkova,[1,2] U. Munari [ID][4] and P. Ochner[3]

[1]*Physics Department, Lomonosov Moscow State University, Leninskie Gory, Moscow 119991, Russia*
[2]*Sternberg Astronomical Institute, Lomonosov Moscow State University, Universitetsky pr.13, Moscow 119234, Russia*
[3]*Department of Physics and Astronomy, Padova University, Vicolo Osservatorio 3, I-35122 Padova, Italy*
[4]*INAF – National Institute of Astrophysics, Astronomical Observatory of Padova, I-36012 Asiago, Italy*

ABSTRACT

Galactic star clusters are known to harbour a significant amount of binary stars, yet their role in the dynamical evolution of the cluster as a whole is not comprehensively understood. We investigated the influence of binary stars on the total mass estimate for the case of the moderately populated Galactic star cluster NGC 225. The analysis of multi-epoch radial velocities of the 29 brightest cluster members, obtained over two observational campaigns, in 1990–1991 and in 2019–2020, yields a value of binary fraction of $\alpha = 0.52$ (15 stars out of 29). Using theoretical isochrones and Monte Carlo simulations we found that the cluster mass increases at least 1.23 times when binaries are properly taken into account. By combining *Gaia* Early Data Release 3 (EDR3) photometric data with our spectroscopic observations, we derived estimates of NGC 225 fundamental parameters as follows: mean radial velocity $\langle V_r \rangle = -9.8 \pm 0.7$ km s^{-1}; $\log(\tau) = 8.0$–8.2 dex; distance $D = 676 \pm 22$ pc; and colour excess $E(B - V) = 0.29 \pm 0.01$ mag.

Key words: techniques: photometric – techniques: radial velocities – open clusters and associations: general – open clusters and associations: individual: NGC 225.

1 INTRODUCTION

Galactic star clusters (open clusters – OCs) represent one of the scales in the hierarchy of star formation and their study does not lose relevance for many crucial reasons, as amply discussed in many recent studies (Cantat-Gaudin et al. 2018). In fact, OCs and associations are the birth place for most stars in the Galactic disc and hence their study makes it possible to trace the evolution not only of individual star-forming regions but also of the disc as a whole (Lada & Lada 2003; Buckner & Froebrich 2013). However, our knowledge of these stellar systems is far from a complete, mostly because of the lack of good quality and statistically significant observational data. For example, reliable mean radial velocities are available for a very small number of open star clusters. This prevents accurate studies of star cluster internal kinematics, dynamics, and chemistry. Besides, it makes it impossible to reconstruct orbits, which in turn is an essential information for studying the kinematics of the disc of the Galaxy, to which the OCs subsystem belongs. High expectations in terms of obtaining accurate radial velocities are associated with the *Gaia* mission, especially with the most recent Data Release 3 (DR3). However, the latest available *Gaia* Early Data Release 3 (EDR3; Gaia Collaboration et al. 2021) inherited *Gaia* Data Release 2 (DR2; Gaia Collaboration et al. 2018) radial velocities, which in most cases are of insufficient precision for determining reliable mean cluster radial velocities. As an example, in the catalogue containing the mean radial velocities for 861 OCs according to *Gaia* DR2 data (Soubiran et al. 2018), for 60 per cent of clusters the estimates of mean radial

velocities are made using three or even fewer stars. In addition, with such small samples of stars having radial velocities it seems challenging to take into account and then study the presence and relevance of binary stars in clusters. From theory, however, we know very well that they play a significant role in the dynamical evolution of the parent cluster: they boost mass segregation, they generate blue stragglers and other exotic system, and, not less important, they are an important source of dynamical heating. Simulations shows that binary systems can be merged and form the most massive stars in the clusters (Oh & Kroupa 2018) or, being massive initially, can be ejected from the parent clusters (Oh et al. 2014; Oh & Kroupa 2016). Along the same vein, their study is therefore important for the correct determination of the cluster mass (Sheikhi et al. 2016) when using virial equilibrium.

The binary fraction (commonly indicate with α) in open star clusters seems to be different than in Galactic globular clusters and in the general Galactic field (Borodina et al. 2019). However, α in the Galactic field apparently relates to the value of binary fraction in open clusters (Kroupa 1995a,1995b,1995c). Theoretical description of the evolution of the binary population in clusters is presented by Marks, Kroupa & Oh (2011). Using dynamical population synthesis Marks & Kroupa (2011) construct the integrated galactic field binary distribution function.

Photometry-based methods remain the most popular way to estimate the binary fraction. The main approach of such studies is to unravel binaries according to their position above the main sequence of the parent cluster colour–magnitude diagram (CMD). Niu, Wang & Fu (2020) used the synthetic CMD method to derive α of 12 OCs, which was found to range from 29 to 55 per cent for

main-sequence stars. Sollima et al. (2010) reported α from 35 to 70 per cent for five OCs using the same method. Also, basing on the stars' position in the CMD, Khalaj & Baumgardt (2013) found binary fraction of 35 per cent for Praesepe (M44) and Sheikhi et al. (2016) reported 34 ± 12 per cent binary fraction for Alpha Persei OC.

Some authors focused on more time-consuming spectroscopy-based methods to unravel binaries by studying radial velocities variations. Geller et al. (2021) summarized their observations of over 45 yr for the old OC M67 and reported an overall $\alpha = 34 \pm 3$ per cent and 70 ± 17 per cent for the cluster centre. On the other hand, Banyard et al. (2022) estimated α to be 52 ± 8 per cent for the B-type stars of the OC NGC 6231.

This study belongs to the latter group of studies. In fact, we aimed at obtaining radial velocities for all cluster members down to a certain magnitude and investigate the binary status of each of them. The OC NGC 225 in Cassiopea is a good target to this aim. It is a moderately populated cluster, located in an uncrowded region ($l \approx 122°0$, $b \approx -1°06$) of the sky. Investigations performed by different authors show very scattered estimates of NGC 225 main physical parameters (Bilir et al. 2016), and in some cases even contradictory. Lattanzi, Massone & Munari (1991) studied NGC 225 and reported estimates of its distance and age of $D = 525 \pm 73$ pc, $\tau = 120$ Myr, respectively. Subramaniam, Mathew & Kartha (2006) claimed that the cluster is much younger, with the $\tau < 10$ Myr and distance $D = 575 \pm 120$ pc. On the contrary, Bilir et al. (2016) reported a larger estimation of age, $\tau = 900 \pm 100$ Myr, with the same distance $D = 585 \pm 20$ pc. Svolopoulos (1962) found a distance $D = 630$ pc. Evaluation of colour excess $E(B - V)$ varies from 0.151 ± 0.047 mag (Bilir et al. 2016) to 0.25 ± 0.08 mag (Lattanzi et al. 1991) and 0.29 mag (Svolopoulos 1962; Subramaniam et al. 2006). The most reliable estimation of mean proper motion in right ascension (RA; $\langle \mu_{\alpha}* \rangle$) and declination (Dec.; $\langle \mu_{\delta} \rangle$) was reported by Cantat-Gaudin et al. (2018) based on *Gaia* DR2 (Gaia Collaboration et al. 2018): $\langle \mu_{\alpha}* \rangle = -5.373$ mas yr^{-1}, $\langle \mu_{\delta} \rangle = -0.093$ mas yr^{-1}; also the most likely distance was derived to be $D = 684.3$ pc.

Mean radial velocities estimations are contradictory too. Bilir et al. (2016) found a mean cluster radial velocity of $\langle V_r \rangle = -8.3 \pm 5$ km s^{-1} from eight stars in the cluster field. Conrad et al. (2017) instead reported $\langle V_r \rangle = 28$ km s^{-1}, whilst Soubiran et al. (2018) used one star to determine mean radial velocity $\langle V_r \rangle = -4.12 \pm 11.13$ km s^{-1}.

Our observational campaigns have therefore a twofold aim. On one side we attempt at amending this large discrepancies in the values of the cluster fundamental parameters. On the other side, we aim at determining its binary fraction and total mass.

To this purpose, the layout of this paper is as follows. Section 2 is dedicated to the selection of cluster members. In Section 3, we describe our observational data. In Section 4, we determine the binary fraction and assess how it affects the mass cluster estimation. Finally, in Section 5, we summarize our results.

2 MEMBERSHIP PROBABILITY

To derive the binary status of each star down to a certain magnitude, the membership probability of the stars should be examined. This step is the very first step of this study and it was performed when only *Gaia* DR2 (Gaia Collaboration et al. 2018) was available. Therefore, we downloaded data from *Gaia* DR2 (Gaia Collaboration et al. 2018) within 25 arcmin radius centred on $\alpha = 0^h43^m31^s$, $\delta = 61°47'43''$. Only data with parallax errors less than 20 per cent were taken into account. In order to distinguish probable cluster

members from field stars, we performed a clustering analysis using the Density-Based Spatial Clustering of Applications with Noise (DBSCAN) algorithm. DBSCAN is a widely used method (Gao 2014; Bhattacharya et al. 2017; Castro-Ginard et al. 2018; Pasquato & Milone 2019; Yalyalieva et al. 2020) that separates all data points into a set of core points in the neighbourhood of each other, non-core points in the neighbourhood of core points, and noise. Two main parameters are needed to be fixed for the clustering analysis using DBSCAN: ϵ – the maximum distance between two points to label that one is in the neighbourhood of the other; and N – the number of points in a neighbourhood of a point to label it as a core point. The algorithm was implemented in the PYTHON language using the library SCIKIT-LEARN (Pedregosa et al. 2011). The clustering was performed in a three-dimensional space using parallaxes and the two components of proper motion. We avoid using positional coordinates because NGC 225 is quite sparse. Before proceeding with the clustering, the coordinates were scaled to unit dispersion and a principal component analysis was performed to exclude possible dependencies between coordinates.

Since it is usually rather complicated to find the best solution for ϵ and N values, we decided to adopt a statistical approach.

As a first step, we examined the vector–point diagram and the parallax distribution of the cluster stars. The bulk proper motion of stars of NGC 225 differs from the mean proper motion of foreground stars significantly. In fact, cluster stars crowd in a clump in vector–point diagram, which is visible even by eye. This clump is centred on the values reported by Cantat-Gaudin et al. (2018) for the cluster proper motion components: $\mu_{\alpha}* \approx -5.4$ mas yr^{-1}, $\mu_{\delta} \approx -0.1$ mas yr^{-1}, where $\mu_{\alpha}* = \mu_{\alpha} \cos\delta$ and μ_{δ}. The stars with proper motion around this values have a mean parallax $\pi \approx 1.4$ mas.

As a second step, we constructed a grid of clustering parameters ϵ and N, extracting them from a wide interval ($\epsilon = 0.01$–0.99, $N = 1$–150), and then we analysed the outcome of the clustering. Among all clustering solutions we selected those variants that produced only two clusters (groups): the group with mean parameters around the values found in the first step (group I), and the field stars group (group II). We found that the $n = 1310$ clustering met this requirements. The number of stars identified as belonging to group I is 183. In a final third step we estimated the probability for a star to belong to NGC 225 by dividing the number of times when a star was related to the group I by the number of all possible clusterings n. The resulting distribution of the membership probability is shown in Fig. 1. According to their probability, we compiled two lists of target stars: stars with probabilities $p > 50$ per cent (List$_{50}$), and stars with $p > 90$ per cent (List$_{90}$) (Fig. 1). Of the 183 stars in group I, 129 have a probability ≥ 0.5 and of these 85 are positioned above the 0.9 threshold. List$_{50}$ is presented in Appendix A (Table A1), where stars are sorted by G_{Gaia} magnitude and labelled from s001 for the brightest stars up to s129 for the faintest one. In the following we adopted stars with membership probability >50 per cent (that is from List$_{50}$), using stars from List$_{90}$ with membership probability >90 for the most reliable estimations or as upper/lower limits.

We compared results of our membership extraction with the list of members identified by Cantat-Gaudin et al. (2018). Cantat-Gaudin et al. (2018) membership list includes 66 stars that lie in the same coordinates' space within ≈ 25 arcmin in radius. We found that all those stars are present in our List$_{50}$ and 62 of them are also present in List$_{90}$.

As a result, following the method we described above, we were able to find the probability for a star to be a cluster member avoiding to search for the exact values of ϵ and N.
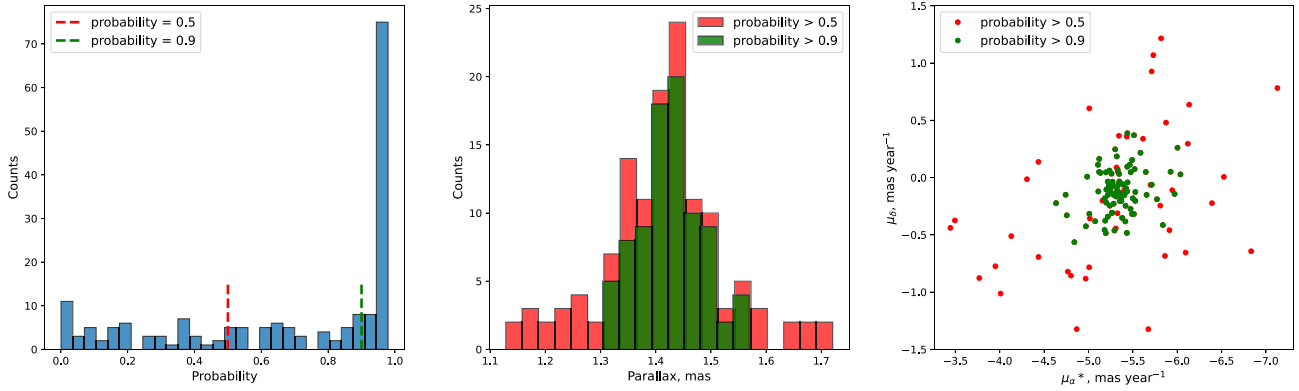
Figure 1. Left-hand panel: distribution of membership probability; probability of all stars ever identified as cluster members is shown. Middle panel: parallax distribution for stars with membership more than 50 per cent (red) and 90 per cent (green). Right-hand panel: proper motion vector–point diagram for stars with membership more than 50 per cent (red) and 90 per cent (green).

Table 1. Summary of mean parameters: mean parallax and its dispersion, mean components of the proper motion in right ascension and declination and corresponding dispersion.

Parameter/membership list	List$_{50}$	List$_{90}$
$\langle \pi \rangle$ (mas)	1.42 ± 0.01	1.43 ± 0.01
$\sigma_{\langle \pi \rangle}$ (mas yr^{-1})	0.10 ± 0.01	0.06 ± 0.01
$\langle \mu_{\alpha}* \rangle$ (mas yr^{-1})	-5.33 ± 0.02	-5.34 ± 0.02
$\sigma_{\langle \mu_{\alpha}* \rangle}$ (mas yr^{-1})	0.46 ± 0.01	0.25 ± 0.01
$\langle \mu_{\delta} \rangle$ mas yr^{-1})	-0.13 ± 0.01	-0.11 ± 0.01
$\sigma_{\langle \mu_{\delta} \rangle}$ (mas yr^{-1})	0.37 ± 0.01	0.20 ± 0.02

In Table 1, the mean values of the parallaxes and proper motions of the member stars are listed. As it may be noticed, the mean values of these two groups are quite similar. One could get the impression that the parallax dispersion is too large (see Fig. 1, middle panel). The maximum difference between the parallax of the star from List$_{50}$ and $\langle \pi \rangle$ is $\Delta_{\pi} = 0.3$ mas, which translates into $\Delta_{\pi}/\langle \pi \rangle^2 = 149$ pc, and a rough estimation for dispersion is $\sigma_{\langle \pi \rangle}/\langle \pi \rangle^2 = 50$ pc. Initially, we adopted data with parallax errors not larger than 20 per cent, which means, again roughly, $0.2 \langle \pi \rangle/\langle \pi \rangle^2 = 141$ pc. This is three times larger than the estimated dispersion and approximately equal to the maximum difference between star parallaxes and $\langle \pi \rangle$. We can therefore conclude that the results of clustering and membership assignment are quite reasonable within the limitations of the input data.

It is important to note, finally, that the 30 brightest stars out of 183 (the whole number of stars ever labelled as group I stars) turned out to have membership probability larger than 50 per cent. Therefore, we are confident we are not going to miss any probable members among the first 30 brightest stars, which corresponds to $G_{\text{Gaia}} \leq 13.4$ mag.

2.1 Differences with *Gaia* EDR3 data

As we performed membership segregation algorithm before *Gaia* Early Data Release 3 (EDR3; Gaia Collaboration et al. 2021), we based our results on *Gaia* DR2 (Gaia Collaboration et al. 2018). To compare our results with the improved data from *Gaia* EDR3, we cross-correlated stars with membership probability >50 per cent with *Gaia* EDR3 data and examined differences between parallaxes and proper motions. For most of the stars from List$_{50}$ the relative

differences between parallaxes from *Gaia* DR2 and *Gaia* EDR3 was less than 10 per cent, and only one star (s051) exhibited a surprisingly significant smaller parallaxes in *Gaia* EDR3 than in *Gaia* DR2 data (difference $(\pi_{\text{DR2}} - \pi_{\text{EDR3}})/\pi_{\text{DR2}} \approx 0.45$ dex). The differences between each proper motion component for most of the stars were within 0.5 mas yr^{-1}, but for the star s051 the difference in μ_{δ} component was two times larger – about 1 mas yr^{-1}. We therefore decided to remove this star from our sample. This change altered only List$_{50}$ and turned the number of the members down to 128.

3 OBSERVATIONS AND DATA REDUCTION

In this study, we used the results of two runs of the observations. Both of them were performed at the Asiago Astrophysical Observatory, Asiago, Italy.

The first series of observations was carried out in 1990–1991 using the 1.8-m Copernico telescope equipped with a Boller and Chivens CCD Spectrograph. The CCD was a coated Thompson TH7882 and the recorded ranges for the 600 and 1200 lines mm^{-1} gratings were $\lambda = 3790$–4910 and 3850–4400 Å, respectively.

The second run was performed in 2019–2020. Observations were conducted with the 122-cm Galileo telescope equipped with the Boller and Chivens CCD Spectrograph with the 1200 lines mm^{-1} grating and range $\lambda = 3820$ 5035 Å. Besides, several echelle spectra ($\lambda = 3470$–7360 Å) were acquired using the 182-cm Copernico telescope.

The reduction of the CCD frames has been done using the IHAP and the IRAF packages. In both series of observations flat-fields have been regularly secured for each observing run, and calibration spectra (Fe/Ar lamp) were recorded before each observation of the target star.

Radial velocities of these two series of observations were extracted in different manner. As for the runs made in 1990–1991, radial velocities have been derived for all target stars with cross-correlation techniques using the routines implemented in the ESO-IHAP software package. The procedure we followed is described in detail in Munari (1992). Briefly, it consists of an iterative process that leads to the definition of a template mean cluster for each observing run that is essentially composed of the normalized and added spectra of all non-binary cluster members. The definition of this template mean cluster has been greatly facilitated by the narrow range of spectral types and projected rotational velocities spanned by NGC 225 target stars. The typical error of the single observation is ≈3 km s^{-1}.

Table 2. Radial velocities of the 29 brightest stars of NGC 225.

Star	Date (dd.mm.yy)	V_r (km s^{-1})	Star	Date (dd.mm.yy)	V_r (km s^{-1})	Star	Date (dd.mm.yy)	V_r (km s^{-1})	Star	Date (dd.mm.yy)	V_r (km s^{-1})
s001	09.01.90	−10	s004	09.01.90	−5	s008	04.12.19	−9.8	s014	23.01.20	−11.8
	17.01.90	−12		17.01.90	−10		22.01.20	−10.3		20.11.20	−10.2
	18.02.90	−5		18.02.90	−8		23.01.20	−9.0	s015	19.02.90	22
	19.02.90	−12		19.02.90	−15		20.11.20	−7.9		28.09.90	−3
	28.09.90	−2		28.09.90	−9		07.02.20^a	−11.1		02.10.90	−15
	02.10.90	−11		14.10.90	0	s009	09.01.90	−9		14.10.90	−8
	14.10.90	−8		08.01.91	−9		18.02.90	−11		06.11.90	25
	06.11.90	−6		24.01.91	−8		19.02.90	−11		08.01.91	4
	08.01.91	−9		25.01.91	−9		28.09.90	−10		26.01.91	−10
	24.01.91	−12		26.01.91	−9		02.10.90	−7		04.12.19	−9.6
	25.01.91	−6		04.12.19	−10.9		14.10.90	−5		22.01.20	−9.7
	26.01.91	−12		22.01.20	−9.3		06.11.90	−2		20.11.20	−9.6
	04.12.19	−9.7		19.11.20	−9.2		08.01.91	−5	s016	12.01.20	−15.8
	11.01.20	−10.4	s005	09.01.90	−5		24.01.91	−3		20.11.20	−12.6
	11.01.20	−12.8		18.02.90	10		26.01.91	−11	s017	04.12.19	−13.9
	19.11.20	−10.3		19.02.90	−10		04.12.19	−9.2		23.01.20	−13.5
s002	09.01.90	−9		28.09.90	−19		22.01.20	−9.9		21.11.20	−12.9
	17.01.90	−8		02.10.90	4		20.11.20	−8.4	s018	12.01.20	−10.1
	18.02.90	−11		14.10.90	−16	s010	04.12.19	−9.4		21.11.20	−11.8
	19.02.90	−8		06.11.90	−28		22.01.20	−11.3	s019	04.12.19	−10.9
	28.09.90	−1		08.01.91	−27		23.01.20	−11.7		23.01.20	−11.9
	02.10.90	−7		24.01.91	−28		20.11.20	−9.3		21.11.20	−10.4
	14.10.90	−5		26.01.91	−10		07.02.20^a	−11.4	s020	04.12.19	−10.8
	06.11.90	−12		04.12.19	−8.3	s011	28.09.90	−1		21.11.20	−10.3
	08.01.91	−13		22.01.20	−11.6		02.10.90	−8	s021	23.01.20	−23.1
	24.01.91	−15		20.11.20	−8.2		14.10.90	−10		21.11.20	−14.5
	25.01.91	−13	s006	19.02.90	−6		06.11.90	1	s022	11.01.20	−9.9
	26.01.91	−8		28.09.90	−10		08.01.91	−20		21.11.20	−10.6
	04.12.19	−8.2		02.10.90	−7		26.01.91	−1	s023	11.01.20	−15.8
	22.01.20	−7.6		14.10.90	−8		04.12.19	−7.1		23.01.20	−15.6
	19.11.20	−8.7		06.11.90	−12		23.01.20	−12.0		21.11.20	−12.7
s003	09.01.90	−5		08.01.91	−6		20.11.20	−12.7	s024	04.12.19	−9.8
	17.01.90	−3		24.01.91	−12	s012	04.12.19	−9.9		21.11.20	−10.4
	18.02.90	−31		04.12.19	−9.8		23.01.20	−11.0	s025	12.01.20	−17.1
	28.09.90	−16		11.01.20	−9.4		20.11.20	−10.3		21.11.20	−13.5
	02.10.90	−3		22.01.20	−9.5		07.02.20^a	−8.3	s026	11.01.20	−15.5
	14.10.90	8		20.11.20	−8.6	s013	09.01.90	−15		21.11.20	−22.3
	06.11.90	−14	s007	09.01.90	−9		28.09.90	−9	s027	11.01.20	−19.5
	08.01.91	−32		28.09.90	1		02.10.90	13		22.11.20	1.2
	24.01.91	−6		02.10.90	−3		14.10.90	10	s028	12.01.20	−6.3
	25.01.91	−2		14.10.90	−9		06.11.90	26		22.11.20	−5.6
	26.01.91	20		06.11.90	−12		08.01.91	30		22.11.20	−5.1
	04.12.19	−4.8		08.01.91	−6		24.01.91	−12	s029	12.01.20	−2.9
	22.01.20	−2.0		24.01.91	1		26.01.91	32		22.11.20	−42.6
	19.11.20	−8.8		26.01.91	−6		04.12.19	−11.4		22.11.20	−41.9
				04.12.19	−9.2		20.11.20	−11.7			
				22.01.20	−9.1						
				20.11.20	−7.6						

Note. ^{a}Refers to echelle observations.

During runs in 2019–2020, to obtain radial velocities from the spectra we used a Fourier cross-correlation technique implemented in IRAF environment. As a template spectra we used synthetic spectra from Munari et al. (2005) with atmospheric parameters appropriate for each spectral type from Aller et al. (1982). Spectral classifications were derived according to Gray & Corbally (2009). Synthetic template spectra for each processing star were then chosen according to the derived spectral classes.

All the data discussed in this study are made public available at the Centre de Données Stellaire data base.

4 PHYSICAL PARAMETERS

4.1 Binary fraction and mean radial velocity

The results of the radial velocities extraction are listed in Table 2, while spectral classification is reported in Table 3.

To single out binary stars, we used the following criteria.

(a) If a star had more than three observations, we used the Pearson's chi-squared test with 95 per cent significance level. This was applied to 11 stars.

Table 3. Spectral classification.

N	Spectral type	Spectral type Lattanzi et al. (1991)
s001	B7	B6.5
s002	B8	B8
s003	B8	B9
s004	B9	A0
s005	B8III	B9
s006	B9	A0
s007	A1	A1
s008	A1	–
s009	A0	A0
s010	A3	A9
s011	A1	A0
s012	A2	–
s013	A1	A3
s014	A2	–
s015	A0III	A2
s016	A3	A5
s017	A5	–
s018	F2	A7
s019	F0	–
s020	F0	A7
s021	A3	
s022	F0	F0
s023	F2	–
s024	F6	F6
s025	F7	
s026	F5	F4
s027	F5	F3
s028	F5	F7
s029	F8	–

Table 4. The number of obtained spectra, mean radial velocity and its dispersion, binary status, and membership probability for the 29 brightest stars in NGC 225.

Star	Number of spectra	$\langle V_r \rangle$ (km s^{-1})	σ_{V_r} (km s^{-1})	Binarity	Membership probability
s001	16	− 9.3	3.1	Single	0.976
s002	15	− 9.0	3.5	Single	0.775
s003	14	− 7.1	13.5	Binary	0.958
s004	13	− 8.6	3.4	Single	0.692
s005	13	− 12.1	11.6	Binary	0.862
s006	11	− 8.9	2.1	Single	0.977
s007	11	− 6.3	4.3	Binary	0.970
s008	5	− 9.6	1.2	Single	0.978
s009	13	− 7.8	3.1	Single	0.977
s010	5	− 10.6	1.2	Single	0.979
s011	9	− 7.9	6.8	Binary	0.979
s012	4	− 9.9	1.2	Single	0.976
s013	10	5.2	19.2	Binary	0.852
s014	2	− 11.0	1.1	Single	0.682
s015	10	− 1.4	14.1	Binary	0.977
s016	2	− 14.2	2.3	Binary	0.955
s017	3	− 13.4	0.5	Binary	0.970
s018	2	− 10.9	1.2	Single	0.845
s019	3	− 11.1	0.8	Single	0.978
s020	2	− 10.6	0.3	Single	0.979
s021	2	− 18.8	6.1	Binary	0.638
s022	2	− 10.3	0.5	Single	0.977
s023	3	− 14.7	1.7	Binary	0.977
s024	2	− 10.1	0.4	Single	0.975
s025	2	− 15.3	2.6	Binary	0.959
s026	2	− 18.9	4.8	Binary	0.977
s027	2	− 9.1	14.6	Binary	0.977
s028	3	− 5.7	0.6	Binary	0.979
s029	3	− 29.1	22.7	Binary	0.977

(b) If a star had only three or two observations, we calculated mean radial velocity (V_r) and dispersion (σ) and then compared them with the cluster mean radial velocity (V_{Cl}) and its dispersion (σ_{Cl}). If V_r differs from V_{Cl} by $3\sigma_{Cl}$ or $\sigma > 3\sigma_{Cl}$, the star was assumed to be a binary.

The mean cluster radial velocity and its dispersion were estimated by means of an iterative process. We used only bona fide single stars. At the first step, we used only stars marked as single by (a) criterion. Then stars marked as single by criterion (b) were added and values of V_{Cl} and σ_{Cl} were calculated again. Iterations were repeated until convergence. The resulting values of mean cluster radial velocity and dispersion are $V_{Cl} = -9.8 \pm 0.7$ km s^{-1}, $\sigma_{Cl} = 1.0 \pm 0.1$ km s^{-1}.

Filtering through (a) and (b) criteria we counted 15 binary stars among 29 stars belonging to the List$_{50}$ or 12 stars among 22 stars belonging to the List$_{90}$, which implies a fraction of binary stars $\alpha = 0.52$ and 0.55, respectively (see Table 4).

4.2 Distance modulus and age

In the next section, we are going to investigate how the obtained value of binary fraction affects the mass estimations of the cluster. We used isochrones to extract from the magnitude of the each star the corresponding mass. To this purpose, we first of all calculated the distance module by fitting with theoretical isochrone the position of member stars in the CMD. The fit was performed eyeballing the stars' distribution in the CMD.

By fitting theoretical PARSEC + COLIBRI isochrones (Bressan et al. 2012) to *Gaia* EDR3 photometry (see Fig. 2), we found the following parameters:

$(m - M)_G = 9.90 \pm 0.06$ mag;

$E(G_{BP} - G_{RP}) = 0.40 \pm 0.02$ mag;

$\log \tau = 8.0$–8.2 dex or 100–160 Myr,

where G_{BP} and G_{RP} are *Gaia* blue and red passbands, see Fig. 2. Using Cardelli, Clayton & Mathis (1989) coefficients we obtained $E(B - V) = 0.29 \pm 0.01$ mag, $(m - M)_0 = 9.15 \pm 0.07$ mag, and distance $D = 676 \pm 22$ pc.

We compared our photometric distance with data from Bailer-Jones et al. (2021), which are based on *Gaia* EDR3 data. Taking the median value of *rgeo* – median of the geometric distance, *b_rgeo* – 16th percentile of the geometric distance, and *B_rgeo* – 84th percentile of the geometric distance, we obtained 682, 664, and 707 pc, respectively. The distance reported by Cantat-Gaudin et al. (2018) is $D = 684.3$ pc. Both values show therefore good agreement with our estimate.

On the other side, our age estimation is in good agreement with the one reported by Lattanzi et al. (1991), namely about 120 Myr.

We derived the same value of the colour excess $E(B - V)$ as in Svolopoulos (1962) and Subramaniam et al. (2006). We compared this value with the data of three-dimensional map of dust reddening (Green et al. 2019). We extracted data in the direction of each star from the List$_{50}$ for the distance of $D = 676$ pc and, assuming $R_v = 3.1$ and using coefficients from Schlafly & Finkbeiner (2011) for conversion, we obtained a mean colour excess of $E(B - V) = 0.29$ mag. Also the three-dimensional medium map STILISM (Capitanio et al. 2017) for the same distance $D = 676$ pc yields a mean colour excess $E(B - V) = 0.31$ mag, in good agreement with the value we obtained.
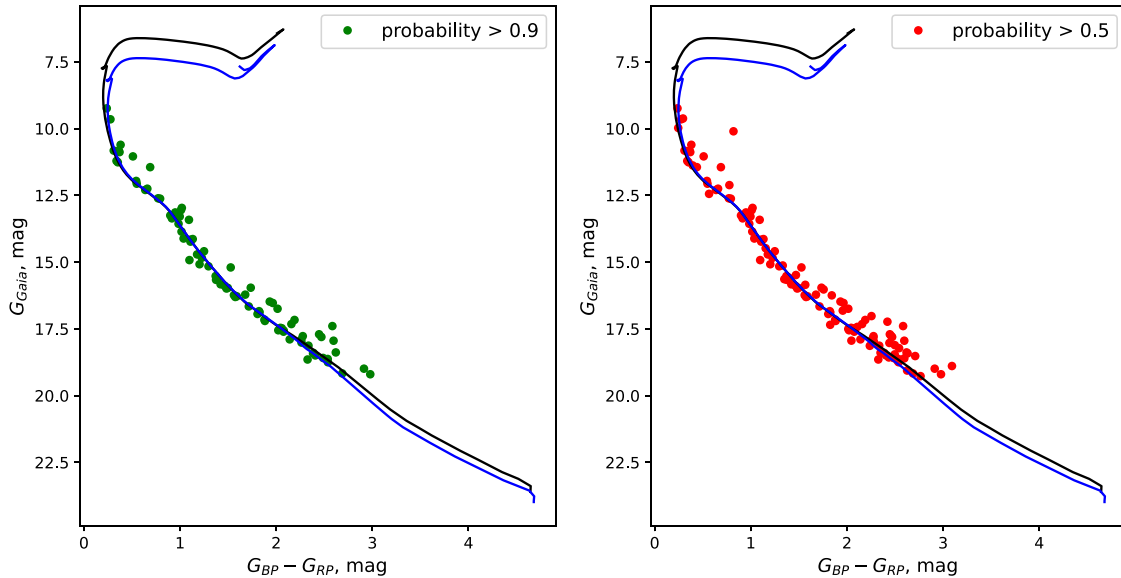
Figure 2. The colour–magnitude diagram (CMD; G_{Gaia}, $G_{BP} - G_{RP}$). Black and blue lines: shifted isochrones with $\log \tau = 8.0$ and 8.2 dex correspondingly. Left-hand panel represents stars with a membership probability greater than 90 per cent, whereas right-hand panel represents stars with a membership probability greater than 50 per cent.
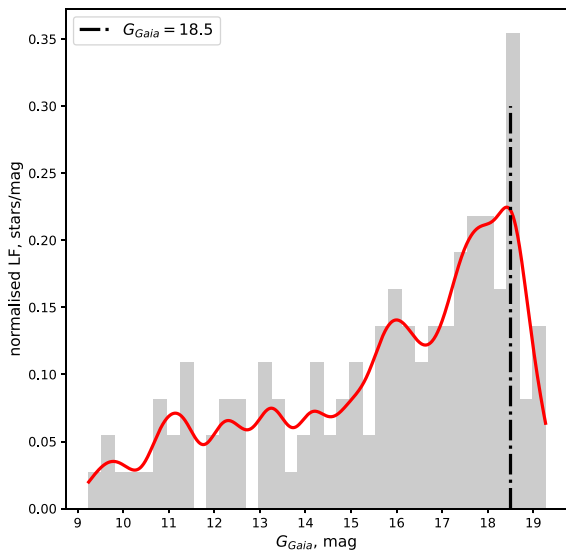

Figure 3. Normalized distribution of *Gaia G* filter for stars with membership probability >50 per cent. Dash–dotted line indicates $G_{Gaia} = 18.5$ mag.

All these results highlight the advantages to perform isochrone fitting when a solid sample of member stars is available.

4.3 Cluster mass

Before calculating the mass of the cluster, it is mandatory to assess the photometric completeness of our sample.

In Boubert & Everall (2020), it is claimed that *Gaia* DR2 is complete down to $G = 18.9$–21.3 mag, depending on the sky coordinates. It seems reasonable to assume that *Gaia* EDR3 limit is not worse than that. In Fig. 3, the normalized distribution of *Gaia* EDR3 *G* magnitude for stars from our List$_{50}$ (membership

probability >50 per cent) is shown. The red line is the output of the kernel density estimator applied to this data. We used Gaussian function as a kernel with a bandwidth = 0.3. We chose this value under the same assumptions as in Seleznev et al. (2017). Below $G_{Gaia} \approx 18.5$ mag a sharp decrease is noticed that we interpreted as photometric completeness limit. In Fig. 3, this limit is indicated with a dashed–dot line. The whole number of stars having $G_{Gaia} \leq 18.5$ mag is 110.

We then estimated the cluster mass by assuming two different values for the binary fraction α.

4.3.1 Binary fraction $\alpha = 0$

In the first case, we assign a binary fraction $\alpha = 0$. To estimate the cluster mass down to $G_{Gaia} = 18.5$ mag, we calculated first the absolute magnitude of each star in G_{Gaia} using $(m - M)_G = 9.90 \pm 0.06$ mag (see Section 4.2). Then we find a transformation function from absolute magnitude to mass $M(G_{Gaia})$ by spline interpolating data from Bressan et al. (2012) isochrones. By summing up the masses of all stars with visual $G_{Gaia} \leqq 18.5$ mag we obtained the cluster mass $\mathcal{M}_0$. Adding and subtracting 0.06 from $(m - M)_G$ we obtained the associated uncertainty. Hence, we get $\mathcal{M}_0 = 126.6 \pm 1.7$ M$_\odot$ for an isochrone with the $\log \tau = 8.0$, and $\mathcal{M}_0 = 125.3 \pm 1.6$ M$_\odot$ for an isochrone with the $\log \tau = 8.2$. The mass that corresponds to $G_{Gaia} = 18.5$ mag is $\mathcal{M}_{lim} = 0.54$ M$_\odot$ for $\log \tau = 8.0$ dex and $\mathcal{M}_{lim} = 0.53$ M$_\odot$ for $\log \tau = 8.2$ dex.

Knowing the distribution of the mass down to $G_{Gaia} = 18.5$ mag, and applying kernel density estimator with Gaussian kernel and bandwidth parameter = 0.2, we constructed the cluster mass function (MF; see Fig. 4). Then, by applying a least-square fit to the logarithmic MF in mass range $0.8 < \mathcal{M} < 1.9$ M$_\odot$, we found the slope coefficient a. Taking into account the uncertainty in $(m - M)_G$ and recalculating the mass of each star according to it for both $\log \tau = 8.0$ and 8.2, we finally obtained $a = -2.53 \pm 0.02$.

We remind the reader that the standard Salpeter initial mass function (IMF) has a slope of $a = -2.35$, while Kroupa (2001)
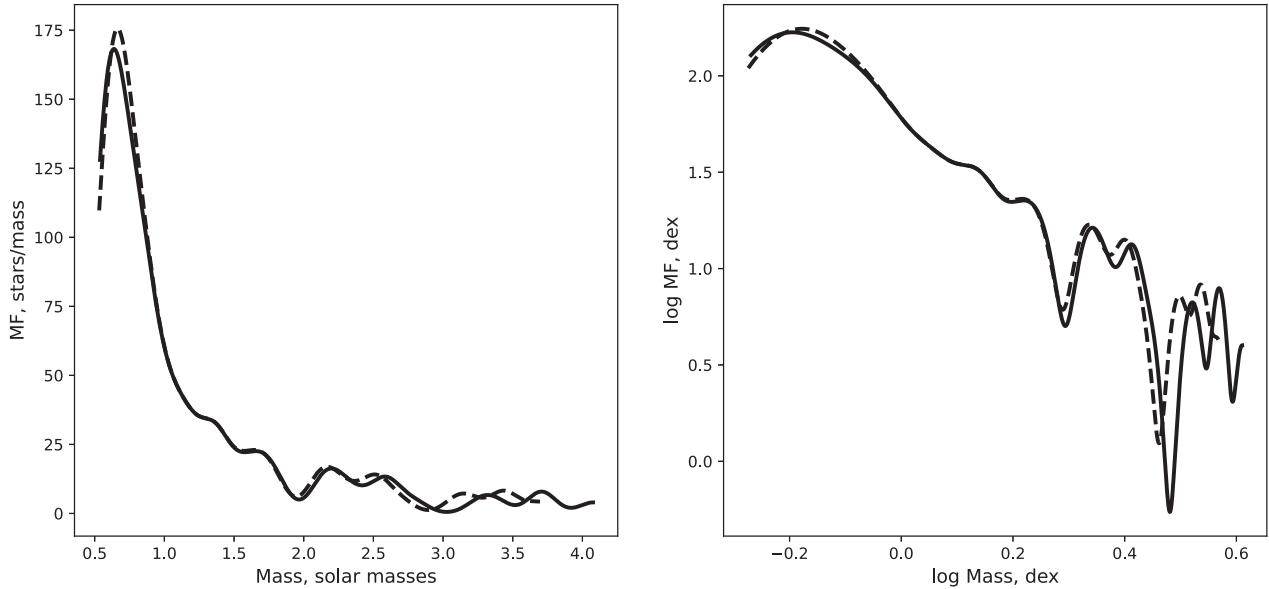
Figure 4. Left-hand panel: mass function, obtained with *Gaia* isochrone $\log \tau = 8.0$ (black line) and $\log \tau = 8.2$ (black dashed line). Right-hand panel: the same as in left-hand panel, but in logarithmic scale.

Table 5. Total cluster mass, its dispersion, and cluster mass increment ν.

Distribution	$\log \tau$ (dex)	$\mathcal{M}_\alpha$ ($M_\odot$)	$\sigma_{\mathcal{M}_\alpha}$ ($M_\odot$)	ν (dex)
$q = 1$	8.0	170.5 ± 2.2	4.5	1.35
	8.2	168.6 ± 2.3	4.8	1.35
Flat distribution	8.0	155.2 ± 2.0	3.7	1.23
	8.2	153.6 ± 1.9	3.6	1.23

proposed $a = -1.3 \pm 0.5$ for stars with mass $0.08 < \mathcal{M} < 0.5\,M_\odot$, $a = -2.3 \pm 0.3$ for $0.5 < \mathcal{M} < 1\,M_\odot$, and $a = -2.3 \pm 0.7$ for mass range $\mathcal{M} > 1\,M_\odot$.

4.3.2 Binary fraction $\alpha = 0.52$

A binary fraction $\alpha = 15/29 \approx 0.517$ is the result that we obtained in Section 4.1 for the stars with membership probability larger than 50 per cent.

We used the same system of equations that were recently used in Borodina et al. (2019), namely:

$$\begin{cases} L = L_1 + L_2, \\ L_1 = L(\mathcal{M}_1), \\ L_2 = L(\mathcal{M}_2), \\ q = \mathcal{M}_2/\mathcal{M}_1, \\ \mathcal{M} = \mathcal{M}_1 + \mathcal{M}_2, \end{cases} \tag{1}$$

where L and $\mathcal{M}$ are the total luminosity and total mass of the binary system, L_1, L_2 and $\mathcal{M}_1$, $\mathcal{M}_2$ are the luminosity and mass of the components, $\mathcal{M}_1 \geqq \mathcal{M}_2$ so $0 < q \leqq 1$.

We also adopted the following equation from Eker et al. (2015):

$$\log L = -0.705 \times (\log \mathcal{M})^2 + 4.655 \times (\log \mathcal{M}) - 0.025. \tag{2}$$

Using isochrones from Bressan et al. (2012) and the distance modulus $(m - M)_G$ previously derived, we transformed *Gaia G* magnitudes into luminosities L. To find a solution for the equation (1) we used

optimization algorithm from the PYTHON library SCIPY (Virtanen et al. 2020) and minimized the following function using a truncated Newton minimization algorithm:

$$y = |L - 10^{L(\mathcal{M}_1)} - 10^{L(q\mathcal{M}_1)}|. \tag{3}$$

Under the assumption that the binary fraction does not depend on the magnitude interval (hence mass), we may consider α as a probability that a randomly chosen star turned out to be a binary. We can therefore assign to each star a value β randomly extracted in the interval [0, 1]. When β turns out to be $\leqq \alpha$ we treat that star as a binary and applied minimization algorithm to find $\mathcal{M}_1$ and then $\mathcal{M} = \mathcal{M}_1 \times (1 + q)$. In the opposite case, we assign to it mass of a single stars as described in Section 4.3.1. Repeating that procedure for 1000 runs, we found mean values of the total cluster mass estimation $\mathcal{M}_\alpha$. Dividing this value by the mass $\mathcal{M}_0$, as calculated in Section 4.3.1, we derived the cluster mass increment ν induced by binaries.

We tested two cases as far as the q distribution is concerned: $q = 1$ and a flat q distribution. In the latter case, after each $\mathcal{M}_1$ calculation we checked whether the value $\mathcal{M}_1 \times q$ is greater than $0.08\,M_\odot$. If this condition was not met, the q value was chosen again. The calculations were done for all the stars with $G_{\text{Gaia}} \leqq 18.5$ mag. Uncertainties in masses were calculated by taking into account uncertainties in distance moduli. The results are listed in Table 5. We emphasize that the difference between the two age values ($\log \tau = 8.0$ dex and $\log \tau = 8.2$ dex) is marginal and well within the uncertainties.

For the case of $q = 1$ we calculated the total mass for the 29 stars for which we had derived the binary status using our spectroscopic criteria. As we had already found binary stars among them, we could calculate their mass in accordance with their binary status and could compare the results obtained for the case of randomly assigned binary stars. The difference did not exceed $4\,M_\odot$ for all cases, or less than 5 per cent.

The obtained cluster mass increments ν are in good agreement with the values obtained by Borodina et al. (2019), where for α

$\approx 0.5\nu$ was found to be about 1.2 for 'realistic' distributions of q, including a flat distribution, and $\nu \approx 1.35$ for $q = 1$.

In this study, we considered only binaries, and not multiple systems. Borodina et al. (2021) demonstrate that taking into account triple and quadruple systems inflates ν significantly. Therefore, our estimations, especially for flat q distribution, should be considered as a lower limit.

5 CONCLUSIONS

In this work, we studied the open star cluster NGC 225 and investigated how the presence of binary stars among cluster members affects the cluster total mass measure. The main results of our study can be summarized as follows.

(1) By using *Gaia* DR2 data and applying a clustering analysis to stars' proper motions and parallaxes, we obtained a list of probable cluster members. All 29 brightest stars from this list have membership probability larger than 50 per cent. By retaining stars with this probability value or larger, we guarantee that the list of bright stars is complete.

(2) We employed spectroscopic observations, collected in 1990–1991 and 2019–2020, and derived radial velocities for the brightest 29 cluster members down to $G = 13.4$ mag in the G *Gaia* EDR3 filter. The binary fraction among this 29 stars turned out to be $\alpha = 0.52$. The mean cluster radial velocity we derived is $\langle V_r \rangle = -9.8 \pm 0.7$ km s^{-1}.

(3) The fit with theoretical isochrones to *Gaia* EDR3 photometric data yields a cluster distance $D = 676 \pm 22$ pc, an age $\log \tau = 8.0$–8.2 dex, and a colour excess $E(B - V) = 0.29 \pm 0.01$ mag.

(4) The cluster mass calculation was performed down to $G_{\mathrm{Gaia}} = 18.5$ mag for two binary fraction values: $\alpha = 0$ and $\alpha = 0.52$ (15 stars out of 29). We used isochrones for mass assignment for single stars, and in the case of $\alpha = 0.52$ we applied Monte Carlo simulations. We tested two types of binary mass distribution: 'flat' and the case of equal mass components. The results of total mass estimations down to $G = 18.5$ mag *Gaia* EDR3 magnitude varies from $\mathcal{M}_0 = 125.3 \pm 1.7\,\mathrm{M}_\odot$ for the case $\alpha = 0$ to $\mathcal{M}_\alpha = 155.2 \pm 2.0\,\mathrm{M}_\odot$ ('flat' mass distribution) and $\mathcal{M}_\alpha = 170.5 \pm 2.2\,\mathrm{M}_\odot$ (equal mass components) for the case $\alpha = 0.52$. The comparison shows that the cluster mass increases between 1.23 and 1.35 times if the binary fraction is taken into account.

DATA AVAILABILITY

The data underlying this paper are available in the paper and in its online supplementary material.

REFERENCES

Aller L. H. et al., 1982, "Landolt-Börnstein: Numerical Data and Functional Relationships in Science and Technology - New Series" Gruppe/Group 6 Astronomy and Astrophysics "Volume 2 Schaifers/Voigt: Astronomy and Astrophysics / Astronomie und Astrophysik" Stars and Star Clusters / Sterne und Sternhaufen. Springer-Verlag, Berlin
Bailer-Jones C. A. L., Rybizki J., Fouesneau M., Demleitner M., Andrae R., 2021, AJ, 161, 147
Banyard G., Sana H., Mahy L., Bodensteiner J., Villaseñor J. I., Evans C. J., 2022, A&A, 658, A69
Bhattacharya S., Mahulkar V., Pandaokar S., Singh P. K., 2017, Astron. Comput., 18, 1
Bilir S. et al., 2016, Adv. Space Res., 58, 1900
Borodina O. I., Carraro G., Seleznev A. F., Danilov V. M., 2021, ApJ, 908, 60
Borodina O. I., Seleznev A. F., Carraro G., Danilov V. M., 2019, ApJ, 874, 127
Boubert D., Everall A., 2020, MNRAS, 497, 4246
Bressan A., Marigo P., Girardi L., Salasnich B., Dal Cero C., Rubele S., Nanni A., 2012, MNRAS, 427, 127
Buckner A. S. M., Froebrich D., 2013, MNRAS, 436, 1465
Cantat-Gaudin T. et al., 2018, A&A, 618, A93
Capitanio L., Lallement R., Vergely J. L., Elyajouri M., Monreal-Ibero A., 2017, A&A, 606, A65
Cardelli J. A., Clayton G. C., Mathis J. S., 1989, ApJ, 345, 245
Castro-Ginard A., Jordi C., Luri X., Julbe F., Morvan M., Balaguer-Núñez L., Cantat-Gaudin T., 2018, A&A, 618, A59
Conrad C. et al., 2017, A&A, 600, A106
Eker Z. et al., 2015, AJ, 149, 131
Gaia Collaboration et al., 2018, A&A, 616, A1
Gaia Collaboration et al., 2021, A&A, 649, A1
Gao X.-H., 2014, Res. Astron. Astrophys., 14, 159
Geller A. M., Mathieu R. D., Latham D. W., Pollack M., Torres G., Leiner E. M., 2021, AJ, 161, 190
Gray R. O., Corbally C. J., 2009, Stellar Spectral Classification. Princeton Univ. Press, Princeton, NJ
Green G. M., Schlafly E., Zucker C., Speagle J. S., Finkbeiner D., 2019, ApJ, 887, 93
Khalaj P., Baumgardt H., 2013, MNRAS, 434, 3236
Kroupa P., 1995a, MNRAS, 277, 1491
Kroupa P., 1995b, MNRAS, 277, 1507
Kroupa P., 1995c, MNRAS, 277, 1522
Kroupa P., 2001, MNRAS, 322, 231
Lada C. J., Lada E. A., 2003, ARA&A, 41, 57
Lattanzi M. G., Massone G., Munari U., 1991, AJ, 102, 177
Marks M., Kroupa P., 2011, MNRAS, 417, 1702
Marks M., Kroupa P., Oh S., 2011, MNRAS, 417, 1684
Munari U., 1992, Mem. Soc. Astron. Ital., 63, 195
Munari U., Sordo R., Castelli F., Zwitter T., 2005, A&A, 442, 1127
Niu H., Wang J., Fu J., 2020, ApJ, 903, 93
Oh S., Kroupa P., 2016, A&A, 590, A107
Oh S., Kroupa P., 2018, MNRAS, 481, 153
Oh S., Kroupa P., Banerjee S., 2014, MNRAS, 437, 4000
Pasquato M., Milone A., 2019, MNRAS, preprint (arXiv:1906.04983)
Pedregosa F. et al., 2011, J. Machine Learning Res., 12, 2825
Schlafly E. F., Finkbeiner D. P., 2011, ApJ, 737, 103
Seleznev A. F., Carraro G., Capuzzo-Dolcetta R., Monaco L., Baume G., 2017, MNRAS, 467, 2517
Sheikhi N., Hasheminia M., Khalaj P., Haghi H., Zonoozi A. H., Baumgardt H., 2016, MNRAS, 457, 1028
Sollima A., Carballo-Bello J. A., Beccari G., Ferraro F. R., Pecci F. F., Lanzoni B., 2010, MNRAS, 401, 577

Soubiran C. et al., 2018, A&A, 619, A155

Subramaniam A., Mathew B., Kartha S. S., 2006, Bull. Astron. Soc. India, 34, 315

Svolopoulos S. N., 1962, ApJ, 136, 788

Virtanen P. et al., 2020, Nat. Methods, 17, 261

Yalyalieva L., Carraro G., Vazquez R., Rizzo L., Glushkova E., Costa E., 2020, MNRAS, 495, 1349

APPENDIX: LIST OF CLUSTER MEMBERS

Table A1. List of cluster members with membership probability >50 per cent. G_{Gaia} magnitude, proper motion, and parallaxes are from *Gaia* DR2.

Star	RA (h:m:s)	Dec. (°:′:″)	G_{Gaia} (mag)	Parallax (mas)	$\mu_\alpha \cos \delta$ (mas yr^{-1})	μ_δ (mas yr^{-1})	Probability	Probability from Cantat-Gaudin et al. (2018)
s001	00:44:40.81	+61:48:43.3	9.2	1.42	− 5.01	− 0.32	0.98	0.2
s002	00:44:30.67	+61:46:49.9	9.6	1.4	− 6.13	0.64	0.77	–
s003	00:44:40.46	+61:54:01.8	9.6	1.32	− 5.42	− 0.13	0.96	–
s004	00:44:46.41	+61:52:31.4	10.0	1.44	− 6.83	− 0.64	0.69	–
s005	00:43:26.58	+61:45:55.7	10.1	1.36	− 5.87	0.48	0.86	0.5
s006	00:43:51.06	+61:50:08.3	10.6	1.41	− 5.24	0.06	0.98	0.8
s007	00:43:51.47	+61:47:13.5	10.8	1.35	− 5.12	0.05	0.97	0.5
s008	00:43:21.88	+61:27:10.7	10.8	1.39	− 5.24	− 0.12	0.98	0.5
s009	00:43:28.88	+61:48:04.0	10.9	1.44	− 5.24	− 0.24	0.98	0.6
s010	00:46:00.67	+61:44:14.5	11.0	1.41	− 5.2	− 0.22	0.98	0.4
s011	00:42:46.90	+61:36:23.0	11.2	1.43	− 5.27	− 0.14	0.98	0.8
s012	00:43:07.74	+61:29:52.3	11.3	1.48	− 5.36	− 0.2	0.98	0.6
s013	00:44:12.81	+61:51:01.8	11.4	1.3	− 5.91	− 0.46	0.85	–
s014	00:40:12.49	+61:41:30.0	11.4	1.49	− 3.95	− 0.77	0.68	–
s015	00:43:25.62	+61:48:51.6	11.5	1.48	− 5.26	− 0.08	0.98	0.7
s016	00:43:36.93	+61:53:40.1	12.0	1.45	− 6.04	0.03	0.95	0.6
s017	00:46:41.32	+61:44:27.4	12.1	1.5	− 5.34	− 0.06	0.97	0.4
s018	00:43:31.00	+61:48:10.1	12.1	1.37	− 4.77	− 0.82	0.85	0.1
s019	00:41:02.54	+61:33:51.5	12.3	1.39	− 5.32	− 0.08	0.98	0.8
s020	00:44:16.53	+61:50:44.0	12.3	1.42	− 5.29	− 0.15	0.98	0.7
s021	00:40:30.79	+61:40:17.5	12.5	1.15	− 5.32	0.09	0.64	–
s022	00:44:11.73	+61:40:16.6	12.6	1.44	− 5.42	− 0.09	0.98	0.8
s023	00:41:35.10	+61:39:42.2	12.6	1.45	− 5.35	− 0.04	0.98	0.8
s024	00:44:20.73	+61:49:45.1	13.0	1.36	− 5.35	− 0.03	0.97	1.0
s025	00:45:25.60	+61:40:23.2	13.1	1.4	− 4.74	− 0.15	0.96	0.1
s026	00:43:18.87	+61:41:14.4	13.2	1.45	− 5.37	− 0.19	0.98	0.9
s027	00:44:47.94	+61:53:38.3	13.3	1.44	− 5.39	− 0.06	0.98	0.9
s028	00:43:05.53	+61:53:43.8	13.3	1.43	− 5.31	− 0.16	0.98	0.7
s029	00:42:50.93	+61:43:21.8	13.4	1.45	− 5.42	− 0.25	0.98	0.9
s030	00:43:25.72	+61:40:31.8	13.4	1.41	− 5.97	− 0.14	0.97	0.5
s031	00:40:52.30	+61:43:14.4	13.6	1.48	− 4.64	− 0.22	0.93	0.1
s032	00:44:14.76	+61:40:21.7	13.9	1.42	− 5.22	− 0.04	0.98	0.7
s033	00:41:14.85	+61:35:30.2	14.0	1.25	− 5.67	− 1.32	0.52	–
s034	00:43:48.95	+61:52:51.8	14.1	1.4	− 5.38	− 0.35	0.98	0.5
s035	00:45:35.25	+61:55:03.4	14.1	1.45	− 5.28	− 0.23	0.98	0.7
s036	00:43:43.35	+61:43:04.5	14.2	1.39	− 5.84	− 0.41	0.96	0.3
s037	00:45:06.51	+61:51:52.7	14.2	1.4	− 5.18	− 0.46	0.97	0.3
s038	00:45:19.99	+61:42:11.4	14.5	1.58	− 5.4	− 0.11	0.88	–
s039	00:45:18.66	+61:55:22.1	14.6	1.52	− 5.66	− 0.15	0.96	0.5
s040	00:41:08.21	+61:49:00.5	14.7	1.43	− 5.33	0.07	0.98	0.8
s041	00:40:37.06	+61:53:53.8	14.9	1.43	− 5.53	− 0.13	0.98	0.8
s042	00:40:12.88	+61:41:31.4	14.9	1.49	− 5.49	0.15	0.97	–
s043	00:45:49.65	+61:42:43.5	15.1	1.39	− 5.48	0.05	0.98	0.8
s044	00:46:07.88	+61:45:06.1	15.1	1.48	− 6.12	0.3	0.89	0.5
s045	00:40:47.91	+61:46:33.6	15.2	1.46	− 5.37	− 0.2	0.98	0.7
s046	00:45:09.60	+61:51:31.3	15.2	1.38	− 5.44	0.1	0.98	0.8
s047	00:45:36.42	+61:57:58.9	15.5	1.42	− 6.39	− 0.22	0.89	–
s048	00:45:08.93	+61:38:36.1	15.5	1.48	− 5.46	0.11	0.97	0.6
s049	00:46:25.80	+61:53:37.6	15.6	1.43	− 3.77	− 0.88	0.64	–
s050	00:40:27.47	+61:46:21.9	15.6	1.42	− 5.44	− 0.04	0.98	0.8
s051	00:44:35.54	+61:25:28.8	15.6	1.33	− 3.44	− 0.44	0.62	–
s052	00:44:46.99	+61:42:53.8	15.7	1.34	− 3.5	− 0.37	0.65	–
s053	00:41:54.71	+61:44:10.5	15.7	1.46	− 5.26	0.03	0.98	0.7
s054	00:40:37.32	+61:57:15.7	15.8	1.47	− 5.39	− 0.06	0.98	0.7

Table A1 – *continued*

Star	RA (h:m:s)	Dec. (°:′:″)	G_{Gaia} (mag)	Parallax (mas)	$\mu_\alpha \cos\delta$ (mas yr^{-1})	μ_δ (mas yr^{-1})	Probability	Probability from Cantat-Gaudin et al. (2018)
s055	00:42:49.15	+62:07:45.6	15.9	1.35	−7.13	0.78	0.51	–
s056	00:41:41.22	+61:53:59.0	15.9	1.36	−4.76	−0.33	0.95	0.1
s057	00:43:35.36	+61:44:31.5	16.0	1.4	−5.35	−0.13	0.98	0.8
s058	00:42:40.78	+61:37:22.3	16.0	1.38	−5.36	−0.16	0.98	0.9
s059	00:40:42.27	+61:36:09.4	16.0	1.44	−5.23	−0.07	0.98	0.5
s060	00:43:16.77	+61:50:15.2	16.1	1.43	−5.82	1.22	0.55	–
s061	00:44:07.20	+62:03:30.4	16.2	1.41	−5.22	−0.15	0.98	0.6
s062	00:42:30.29	+61:40:47.7	16.3	1.4	−5.53	−0.2	0.98	0.8
s063	00:43:14.64	+62:09:21.2	16.3	1.24	−4.44	0.14	0.72	–
s064	00:40:31.44	+61:56:55.0	16.3	1.33	−5.71	−0.06	0.96	–
s065	00:42:21.24	+61:39:43.0	16.3	1.42	−5.32	−0.12	0.98	0.7
s066	00:41:15.67	+61:31:05.9	16.5	1.56	−5.34	0.03	0.91	–
s067	00:43:15.29	+62:07:26.1	16.5	1.34	−5.59	0.22	0.95	0.5
s068	00:43:55.29	+61:52:38.6	16.5	1.57	−5.14	0.04	0.9	–
s069	00:44:09.51	+61:42:54.9	16.7	1.35	−5.18	−0.18	0.97	0.4
s070	00:44:05.50	+62:02:13.8	16.8	1.43	−5.65	0.05	0.98	0.7
s071	00:42:41.18	+61:49:10.1	16.8	1.45	−5.73	1.07	0.65	–
s072	00:44:24.93	+61:49:58.5	16.9	1.51	−5.3	0.25	0.95	0.5
s073	00:44:17.30	+61:55:07.7	16.9	1.4	−5.4	−0.15	0.98	0.7
s074	00:41:50.85	+61:58:22.4	17.0	1.43	−5.27	−0.04	0.98	0.4
s075	00:44:10.57	+62:02:03.7	17.0	1.36	−4.01	−1.01	0.66	–
s076	00:45:06.70	+61:37:39.5	17.2	1.38	−5.77	−0.19	0.97	0.4
s077	00:43:47.32	+62:05:31.0	17.2	1.7	−4.31	−0.01	0.5	–
s078	00:42:31.63	+61:45:30.6	17.2	1.42	−5.5	−0.18	0.98	0.6
s079	00:42:30.56	+61:32:27.6	17.2	1.55	−5.49	−0.32	0.92	–
s080	00:43:03.84	+61:45:32.4	17.3	1.45	−6.0	0.26	0.94	0.6
s081	00:43:05.72	+61:39:49.6	17.4	1.17	−6.53	0.01	0.55	–
s082	00:43:28.66	+61:49:18.5	17.4	1.38	−5.2	−0.1	0.98	0.5
s083	00:45:42.85	+61:38:36.2	17.4	1.36	−5.01	0.6	0.81	0.1
s084	00:43:16.66	+61:49:09.3	17.5	1.54	−5.11	0.11	0.93	–
s085	00:46:15.54	+61:41:18.6	17.5	1.51	−5.12	0.16	0.96	0.4
s086	00:40:46.66	+61:43:58.5	17.5	1.27	−5.16	−0.2	0.89	–
s087	00:41:22.97	+61:47:53.4	17.6	1.38	−5.27	−0.06	0.98	0.6
s088	00:44:44.44	+61:42:58.5	17.6	1.5	−5.22	−0.34	0.97	0.5
s089	00:40:16.25	+61:50:39.7	17.6	1.46	−5.42	−0.38	0.98	–
s090	00:43:53.48	+61:43:42.8	17.7	1.44	−5.44	0.39	0.95	0.4
s091	00:42:57.00	+61:54:40.7	17.8	1.54	−5.71	0.93	0.62	–
s092	00:42:45.07	+61:48:03.7	17.8	1.36	−4.84	−0.56	0.92	0.2
s093	00:43:25.87	+61:39:56.7	17.8	1.59	−5.33	0.05	0.88	–
s094	00:44:49.01	+61:47:40.1	17.8	1.3	−5.52	0.07	0.93	–
s095	00:41:02.70	+61:31:45.3	17.9	1.32	−4.97	−0.42	0.91	–
s096	00:44:10.38	+61:47:25.8	17.9	1.51	−5.47	−0.27	0.97	0.5
s097	00:44:54.76	+61:40:56.6	17.9	1.17	−5.31	−0.44	0.67	–
s098	00:42:45.38	+61:46:45.1	18.0	1.39	−5.51	0.37	0.95	0.4
s099	00:42:26.85	+61:54:00.4	18.0	1.22	−5.26	−0.31	0.77	–
s100	00:40:56.82	+61:57:39.0	18.0	1.35	−5.44	−0.12	0.97	–
s101	00:42:11.84	+61:34:43.9	18.1	1.65	−4.44	−0.69	0.56	–
s102	00:42:08.48	+61:55:57.5	18.1	1.55	−5.43	0.36	0.88	–
s103	00:41:34.23	+61:29:19.6	18.2	1.41	−5.27	−0.31	0.98	–
s104	00:46:24.32	+61:53:44.3	18.2	1.33	−4.87	−1.32	0.62	–
s105	00:43:28.66	+61:47:18.7	18.3	1.44	−4.8	−0.86	0.85	–
s106	00:44:04.17	+61:53:30.2	18.4	1.46	−5.92	0.05	0.96	–
s107	00:46:55.77	+61:43:46.2	18.4	1.49	−5.2	−0.48	0.96	–
s108	00:44:17.22	+61:50:32.7	18.4	1.21	−5.33	−0.31	0.77	–
s109	00:44:17.00	+61:43:21.0	18.4	1.64	−5.34	0.36	0.69	–
s110	00:42:50.68	+61:48:46.0	18.5	1.49	−5.11	−0.12	0.97	–
s111	00:42:13.88	+61:57:02.0	18.5	1.13	−5.27	−0.31	0.6	–
s112	00:46:16.24	+61:32:28.7	18.5	1.49	−5.08	−0.38	0.97	–
s113	00:42:13.54	+61:59:10.7	18.5	1.25	−5.61	0.34	0.8	–
s114	00:44:46.60	+61:44:02.6	18.6	1.59	−5.7	−0.06	0.86	–
s115	00:44:26.51	+61:47:43.8	18.6	1.72	−5.02	−0.36	0.53	–
s116	00:43:46.04	+61:58:12.1	18.6	1.22	−5.86	−0.68	0.68	–

Table A1 – *continued*

Star	RA (ʰ:ᵐ:ˢ)	Dec. (°:′:″)	G_{Gaia} (mag)	Parallax (mas)	$\mu_\alpha \cos\delta$ (mas yr^{-1})	μ_δ (mas yr^{-1})	Probability	Probability from Cantat-Gaudin et al. (2018)
s117	00:43:34.31	+62:11:00.3	18.6	1.44	− 5.19	− 0.38	0.98	–
s118	00:47:04.85	+61:41:07.8	18.6	1.28	− 4.13	− 0.51	0.73	–
s119	00:43:47.53	+61:53:27.5	18.6	1.36	− 4.99	0.01	0.97	–
s120	00:44:20.64	+61:45:45.6	18.7	1.33	− 5.2	0.05	0.96	–
s121	00:44:30.13	+61:46:20.2	18.7	1.17	− 5.94	− 0.11	0.66	–
s122	00:41:25.27	+61:37:41.5	18.7	1.32	− 5.01	− 0.78	0.83	–
s123	00:45:09.05	+61:41:49.0	18.8	1.44	− 5.51	− 0.32	0.98	–
s124	00:44:18.79	+62:03:44.7	18.9	1.25	− 4.97	− 0.88	0.71	–
s125	00:46:21.85	+61:48:37.8	19.0	1.44	− 5.32	0.18	0.97	–
s126	00:45:45.89	+61:29:46.5	19.1	1.68	− 5.81	− 0.24	0.61	–
s127	00:44:48.58	+61:34:29.6	19.2	1.35	− 5.43	− 0.48	0.95	–
s128	00:44:54.27	+61:50:36.5	19.2	1.52	− 5.29	− 0.46	0.94	–
s129	00:42:49.29	+61:59:25.9	19.3	1.68	− 6.1	− 0.66	0.56	–

This paper has been typeset from a TEX/LATEX file prepared by the author.